SUPPORTING INFORMATION, Note S1

Experimental method

Fluorine-doped tin oxide (FTO) coated conductive glass (Asahi-DU, 10 Ω/sq.) used as the substrate was mounted to a home-made rotating disk electrode (RDE) set up via a cylindrical attachment, to which a masking tape (Nitto Denko N-380) with a concentric round hole was attached to regulate the circular active area to 1.54 cm^2. The use of RDE is essential to obtain homogeneous thin films with a high reproducibility as the electrodeposition of ZnO by ORR takes place close to the diffusion limit of O_2.[S1] Potentiostatic electrolysis at -1.0 V vs. Ag/AgCl, under O_2 atmosphere, 70°C, ω = 500 rpm for 10 minutes yielded thin film samples, in aqueous solutions containing 5 mM zinc chloride ($ZnCl_2$, 98%, Merck), 50 mM potassium chloride (KCl, 99.5%, Kanto) and with (up to 500 μM) or without added 2,5-dihydroxy terephthalic acid (DHTPA, $C_8H_6O_6$, 98%, TCI). The pH of solutions was adjusted to 6.00 with small amount of concentrated KOH/HCl aqueous solution. The product thin films were rinsed with water, dried under air at room temperature.

The amount of electrodeposited ZnO or $Zn(OH)_2$ in some cases was estimated from the amount of Zn^{2+} ions as analyzed by an inductively coupled plasma mass spectroscopy (ICP-MS, Perkin-Elmer, ELAN DRC II) for 10 mL of 1 mol dm^{-3} HCl dissolving the entire film. The Faradic efficiencies were then determined according to the overall stoichiometry as,

$$Zn^{2+} + 1/2O_2 + 2e^- \rightarrow ZnO \quad (1)$$

$$Zn^{2+} + 1/2O_2 + H_2O + 2e^- \rightarrow Zn(OH)_2 \quad (2)$$

The amount of DHTPA loaded into the film was determined by measuring the absorption spectra on a UV-Vis spectrophotometer (Shimadzu, SolidSpec-3700). XRD patterns of the thin film samples were measured on an X-ray diffractometer (Rigaku, SmartLab) using Cu Kα radiation. Surface morphology of the electrodeposited thin films was observed on a scanning electron microscope (SEM, JEOL, JSM-IT800). Fourier-transform infrared (FTIR) spectra (JASCO, FT/IR-4700) were measured for both the DHTPA powder and the ZnO/DHTPA hybrid films. Measurements of DHTPA powder were made by mixing it with dried KBr pressing it into a transparent pellet. Attenuated total reflection (ATR)-FTIR spectra of the ZnO/DHTPA hybrid films were measured directly on films electrodeposited on FTO glass at –1.0 V vs. Ag/AgCl for 20 min from an O_2-saturated aqueous solution containing 5 mM $ZnCl_2$, 50 mM KCl, and 0–500 μM DHTPA. Spectra were measured from 1000–3500 cm^{-1} with 4 cm^{-1} resolution by averaging 128 scans.

The redox behavior of the electrodeposited ZnO/DHTPA thin films was studied in sulfate-based, near-neutral electrolyte aqueous solutions under N_2 at room temperature. The measurements were carried out in a three-electrode setup, with a Pt plate as a counter and an Ag/AgCl as a reference electrode in a single compartment cell, and employing a Biologic VMP3 potentiostat controlled by *EC-Lab*® software. Cyclic voltammograms (CVs) were measured at a scan rate in the range between 5 and 100 mV s^{-1} in a 1.0 M Na_2SO_4 neutral aqueous solution or those whose pH was adjusted between 4 and 10 by adding a small amount of 1 M H_2SO_4 or 1 M NaOH.

Electrodeposition was performed at least three times and electrochemical characterization of thin films was performed twice.

Methods to determine the values plotted in Figure 2

The amount of electrodeposited ZnO (mol cm^{-2}) was calculated from the amount of Zn^{2+} ion in 10 mL of 1 mol dm^{-3} HCl solutions dissolving the entire film (projected area = 1.54 cm^2) as analyzed by ICP-MS. Assuming the stoichiometry for the formation of ZnO as:

$$Zn^{2+} + O_2 + H_2O + 2e^- \rightarrow ZnO + H_2O_2 \quad (3)$$

We calculated the Faradic efficiency by comparison to the passed charge according to:

$$Faradaic\ efficiency\ for\ ZnO\ formation\ [\%] = \frac{F\ [C\ mol^{-1}] \times n \times Amount\ of\ electrodeposited\ ZnO\ [mol\ cm^{-2}] \times Electrode\ area\ [cm^2] \times 100}{Passed\ charge\ [C]} \#(4)$$

The amount of DHTPA loaded into the film (mol cm^{-2}) was determined from the UV-Vis absorption spectra of the solutions dissolving the films as above. DHTPA exhibits a sharp absorption peak in the UV range, at λ = 365 nm with a molar extinction coefficient ε = 4,400 M^{-1} cm^{-1} (in 1 M HCl). The solutions dissolving the hybrid thin films exhibit this absorption peak as below (Figure S1).

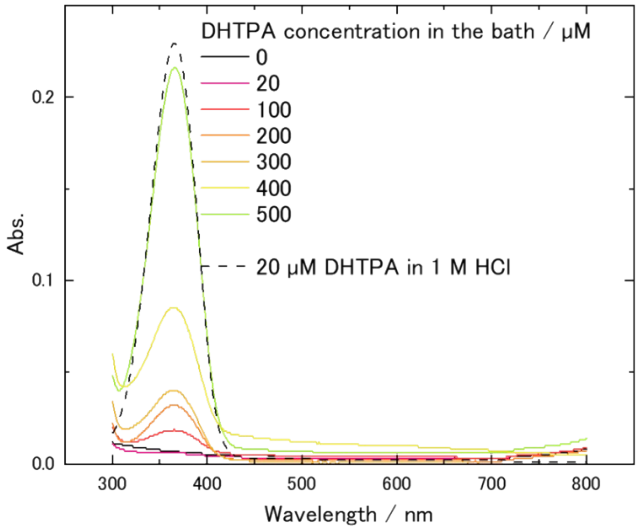

Figure S1 Absorption spectra of 1 M HCl solutions dissolving the electrodeposited thin films with 0, 20, 100, 200, 300, 400 and 500 μM DHTPA at -1.00 V vs. Ag/AgCl for 10 min, in comparison with 20 μM DHTPA in 1 M HCl.

Thus, the DHTPA loading can be calculated from the absorbance (A) according to Lambert-Beer's law as,

$$DHTPA\ loaded\ into\ the\ film\ [mol\ cm^{-2}] = \frac{A \times Volume\ of\ solution\ [L]}{\varepsilon\ [L\ mol^{-1}\ cm^{-1}] \times L\ [cm] \times Electrode\ area\ [cm^2]} \#(5)$$

Optical cells with a long path length (L) and small volume of 1 M HCl were appropriately used for the thin films with a small content of DHTPA to improve the precision of the analysis.

Having known the molar amount of ZnO and DHTPA, their molar ratio in the hybrid thin film can simply be expressed by,

$$Molar\ ratio\ of DHTPA/ZnO\ [-] = \frac{DHTPA\ loaded\ into\ the\ film\ [mol\ cm^{-2}]}{Amount\ of\ electrodeposited\ ZnO\ [mol\ cm^{-2}]} \#(6)$$

One can also estimate the volume ratio occupied by each one of these components. The formular weight and density of ZnO are FW (ZnO) = 81.38 g mol^{-1} and ρ (ZnO) = 5.61 g cm^{-3}, respectively. While the molecular weight of DHTPA is MW (DHTPA) = 198.18 g mol^{-1}, its density was not available from literature. Since those of terephthalic acid and hydroquinone are 1.52 and 1.33 g cm^{-3}, respectively, the central value of ρ (DHTPA) = 1.43 g cm^{-3} was assumed.

By taking the above values, the volume ratio of those occupied by ZnO and DHTPA can be estimated, although not all of Zn may be precipitated as ZnO but partly as $Zn(OH)_2$. The volume ratio of DHTPA/ZnO is thus calculated as,

$$Volume\ ratio\ of DHTPA/ZnO\ [-]$$

$$= \frac{DHTPA\ loaded\ into\ the\ film\ [mol\ cm^{-2}] \times MW(DHTPA)[g\ mol^{-1}] \times \rho(ZnO)\ [g\ cm^{-3}]}{Amount\ of\ electrodeposited\ ZnO\ [mol\ cm^{-2}] \times FW(ZnO)\ [g\ mol^{-1}] \times \rho(DHTPA)[g\ cm^{-3}]} \#(7)$$

These values are plotted in Figure 2 to envision the structure of the hybrid thin films.

Methods for Density Functional Theory Calculations

We performed density functional theory (DFT) calculations using the *Gaussian 16* software package. We compared three functionals as shown in Table S1 and harmonic vibrational frequencies were scaled by a factor of 0.97 for B3LYP and CAM-B3LYP, and 0.95 for the M06 functional, to correct for systematic overestimation inherent to DFT [S2, S3]. We chose the CAM-B3LYP functional in subsequent calculations to more accurately capture charge-transfer interactions and long-range polarization effects [S4, S5]. For most calculations, we applied the 6-311+G(d,p) basis set, which offers a balanced treatment of valence and polarization through the inclusion of diffuse functions that are essential for describing charge delocalization and weak non-covalent interactions at the polymer–ZnO interface [S6]. When geometry optimizations yielded imaginary frequencies, we switched to the def2-TZVP basis set to enhance numerical stability and provide a more complete representation of polarization and metal–ligand interactions. Two negative frequencies are still observed in the monodentate bridge model, suggesting that further optimization may be required to reach a global energy minimum.

Assignment	Experimental (cm^{-1})	B3LYP (cm^{-1})	CAM-B3LYP (cm^{-1})	M06 (cm^{-1})
ν_{asym}(COOH)	1651	1709	1759	1726
δ(CH), ν_{ring}(C=C)	1497	1500	1528	1478
δ (OH), ν_{ring}(C=C), ν(COOH)	1430	1417	1450	1412
δ(CH), δ(OH), ν_{ring}(C=C), ν_{asym}(COOH)	1360	1322	1315	1315
δ (CH), δ (OH)	1291	1225	1235	1201

Table S1 Experimental and scaled DFT-calculated IR frequencies for DHTPA powder obtained using B3LYP (0.97), CAM-B3LYP (0.97), and M06 (0.95) functionals using a 6-311+G(d,p) basis.

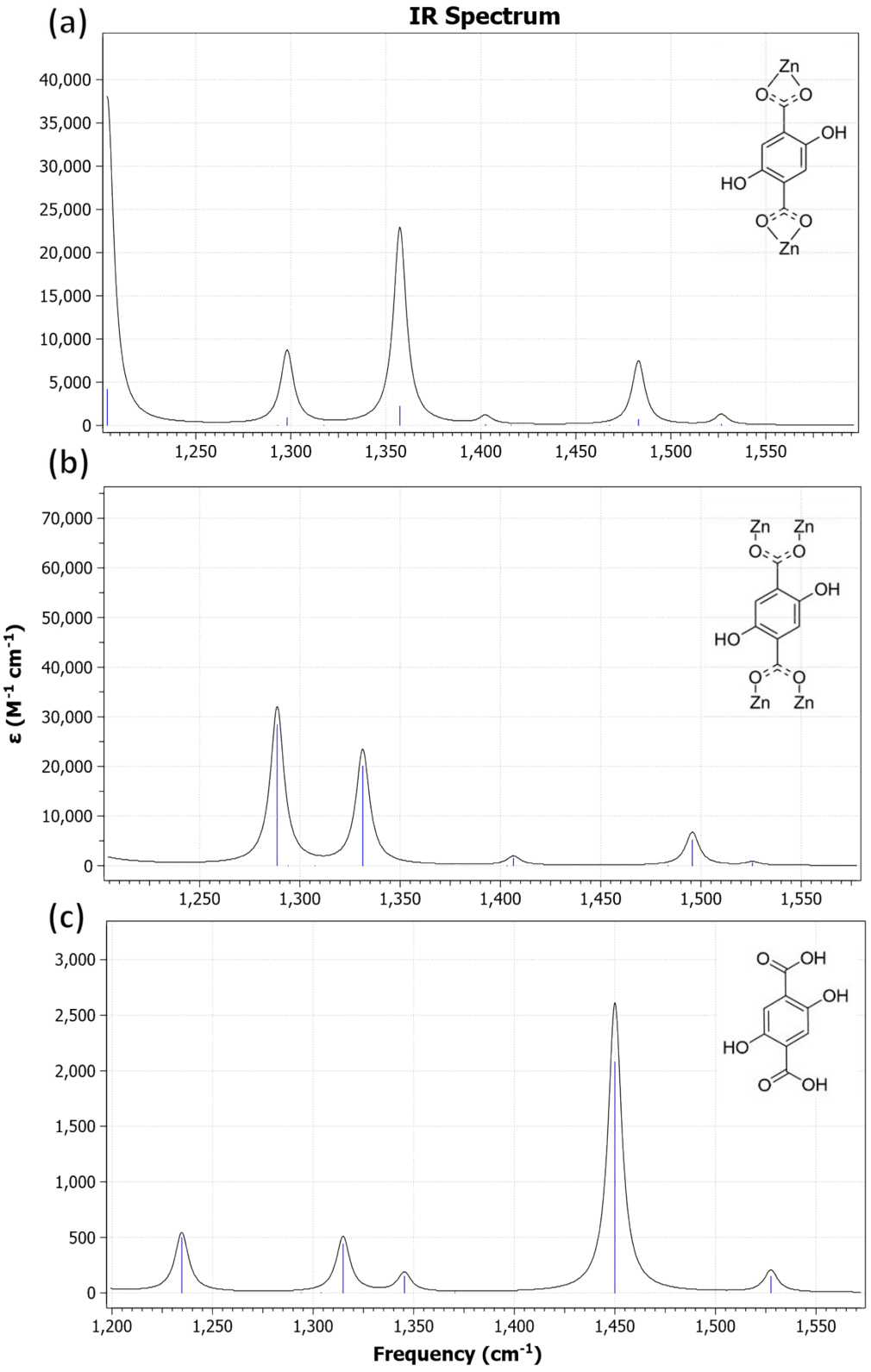

Figure S2 Theoretical IR spectra of (a) DHTPA chelated to a Zn atom, (b) DHTPA monodentate bridging with two Zn atoms and (c) DHTPA solid, computed using CAM-B3LYP and a 6-311+G(d,p) basis. Frequencies are scaled by a factor of 0.97.

DFT Band Assignment	DHTPA Solid Exp (cm^{-1})	DHTPA Solid DFT (cm^{-1})	DHTPA @ 200 µM (cm^{-1})	DHTPA @ 500 µM (cm^{-1})	DHTPA Monodentate Bridge DFT (cm^{-1})	DHTPA Chelated DFT (cm^{-1})
ν_{asym}(COOH)	1651	1753	-	-	-	-
δ(CH), ν_{ring}(C=C)	1497	1528	-	-	-	-
δ (OH), ν_{ring}(C=C), ν(COOH)	1430	1450	-	-	-	-
δ(CH), δ(OH), ν_{ring}(C=C), ν_{asym}(COO-)	-	-	1564	1541	1526*	1527*
δ(CH), δ(OH), ν_{ring}(C=C), ν_{asym}(COO-)	-	-	1564	1541	1496*	1483*
δ(CH), δ(OH), ν_{ring}(C=C), ν_{sym}(COO-)	-	-	1398	1414	1407**	1403**
δ(CH), δ(OH), ν_{ring}(C=C), ν_{sym}(COO-)	-	-	1398	1414	1331**	1357**
δ(CH), δ(OH), ν_{ring}(C=C), ν_{asym}(COOH)	1360	1315	-	-	-	-
δ(CH), δ(OH)	1291	-	-	-	1289	1298

*Polymerization of DHTPA results in significantly broadened IR bands. Therefore, we assign the 1564/1541 cm^{-1} bands in the experimental spectra to both the predicted 1526/1496 cm^{-1} and 1527/1483 cm^{-1} modes of the monodentate bridge and chelate structures, respectively.

**Polymerization of DHTPA results in significantly broadened IR bands. Therefore, we assign the 1398/1414 cm^{-1} bands in the experimental spectra to both the predicted 1407/1331 cm^{-1} and 1403/1357 cm^{-1} modes of the monodentate bridge and chelate structures, respectively.

Table S2 DFT-predicated IR frequencies for chelated and monodentate bridge coordination geometries compared to experimental frequencies of 200 and 500 µM DHTPA thin-film and DHTPA solid. The CAM-B3LYP functional was used and frequencies scaled by 0.97.

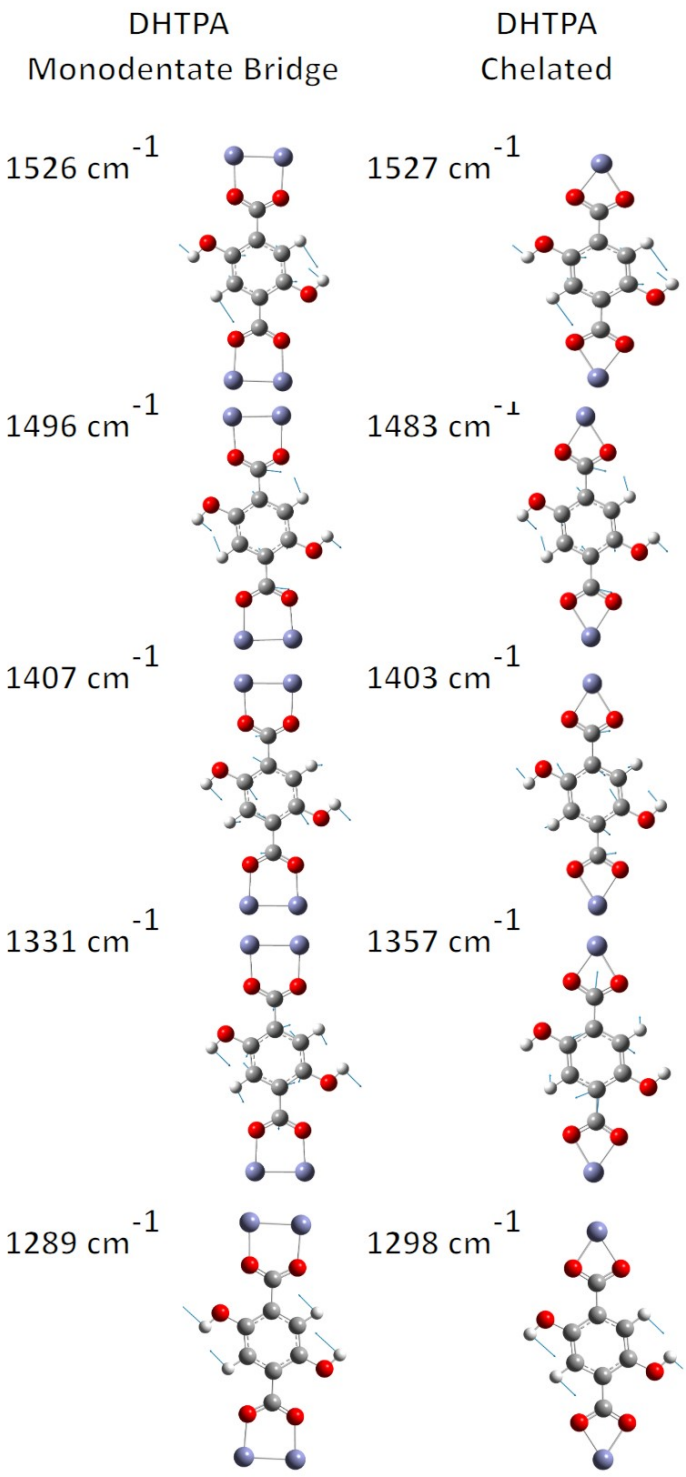

Figure S3 Vibrational modes predicted by DFT calculations for the chelated and monodentate bridge coordination geometries of the DHTPA bound to the surface of ZnO. The CAM-B3LYP functional was used, and frequencies were scaled by 0.97.

Reference

S1 A. Goux, T. Pauporté and D. Lincot, *Electrochim. Acta*, 2006, 51, 3168-3172.

S2 J. Chem. Theory Comput. 2010, 6, 9, 2872–2887

S3 Alecu, I.; Zheng, J.; Zhao, Y.; Truhlar, D. G. J. Chem. Theory Comput. 2010, *6* (9), 2872–2887

S4 Yanai, T.; Tew, D. P.; Handy, N. C. Chem. Phys. Lett. 2004, *393* (1–3), 51–57

S5 Saporiti, G.; Ciammaruchi, L.; Pavone, M.; Barone, V. J. Phys. Chem. C 2024, *128* (10), 4624–4637.

S6 Bursch, M.; Mewes, J.-M.; Hansen, A.; Grimme, S. Angew. Chem. Int. Ed. 2022, *61*, e202205735.